Journal of Materials Chemistry A

Accepted Manuscript

ROYAL SOCIETY OF CHEMISTRY

www.rsc.org/materialsA

Journal Name

COMMUNICATION

Porous $Na_3V_2(PO_4)_3$@C Nanoparticles Enwrapped in Three-dimensional Graphene for High Performance Sodium-Ion Batteries†

Received 00th January 20xx,
Accepted 00th January 20xx

DOI: 10.1039/x0xx00000x
www.rsc.org/

Junqi Fang,[a] Suqing Wang*,[a], Zhitong Li,[a] Hongbin Chen,[a] Lu Xia,[a] Liangxin Ding[a] and Haihui Wang*,[a,b]

Porous $Na_3V_2(PO_4)_3$@C nanocomposites enwrapped in a 3D graphene network was prepared using a simple freeze-drying-assisted thermal treatment method. The carbon layer and 3D graphene network provide not only a 3D conductive network but also a double restriction on the aggregation of $Na_3V_2(PO_4)_3$ particles that have a high crystallinity under high temperature treatment. Due to the high electrochemical activity of the highly crystalline $Na_3V_2(PO_4)_3$ nanoparticles and 3D conductive network, the novel NVP@C/G material displays a superior rate capability (76 mAh g^{-1} at 60 C) and ultralong cyclability (82% capacity retention for 1500 cycles at 40 C) when used in sodium-ion batteries.

Introduction

Due to the resource shortage and environmental issues, sodium-ion batteries (SIBs) are widely considered to be an excellent choice for next-generation hybrid electric vehicles and large-scale energy storage equipment. In particular, the sodium-containing resource is abundant in nature. Furthermore, sodium has similar physical and chemical properties as lithium; thus, the established theories for lithium-ion batteries (LIBs) could apply to SIBs.[1-5] SIBs are promising substitutes for LIBs, which have been industrialized.[6-8] However, it is still a significant challenge to finding suitable electrode materials that have the same storage capacity and cyclability as LIBs. This is due to the larger ionic radius of Na^+ compared with Li^+ (results in a low ion diffusion coefficient)[5] and the serious structure degradation during the intercalation/deintercalation procedure, resulting in poor cyclability and rate capability.[9] Therefore, it is necessary to find suitable electrode materials with a long cyclability and outstanding rate capability for SIBs.

Currently, various cathode materials, such as $NaFeF_3$,[10] $FePO_4$,[11] $NaMPO_4$,[12,13] Na_xMO_2,[14] $Na_3M_2(PO_4)_2F_3$[15] and V_2O_5,[16,17] have been extensively studied. Among these, $Na_3V_2(PO_4)_3$ (NVP) is a typical NASICON framework with large tunnels that has an excellent ionic conductivity and good thermal stability. Additionally, as a cathode material, NVP has a voltage plateau of approximately 3.4 V, and the theoretical energy density is impressive (400 Wh kg^{-1}, 117 mAh g^{-1}× 3.4 V for the V^{3+}/V^{4+} redox couple).[18,19] All of the above advantages make NVP a promising cathode material for SIBs. Unfortunately, the low electrical conductivity of NVP significantly limits its electrochemical performance, especially for the rate capability. Furthermore, the typical synthetic methods to produce NVP usually involve high temperature calcinations that yield micron-sized particles (>2 μm).[20-23] Jian et al. synthesized NVP/C at 900 °C, and the obtained NVP composites only delivered 29 mAh g^{-1} at 1 C.[20] Song et al. reported a NVP prepared via a solution-based carbothermal reduction method that delivered 80 mAh g^{-1} at 2 C.[23] The poor rate capacity was caused by the large particle size of the NVP particles with a low conductivity.

To overcome these issues, many approaches have been attempted to improve the electrochemical performance of NVP. These include the following: (i) decreasing the particle size to the nanoscale level to shorten the Na^+ diffusion distance. Saravanan et al. synthesized nano-sized NVP particles at 650 °C, and the NVP nanoparticles exhibited a superior rate capability (62 mAh g^{-1} at 40 C).[18] Usually, a low calcination temperature (<750°C) is chosen to keep the particle size on the nanoscale, but this results in a low crystallinity of the NVP particles, which would affect the electrochemical performance, especially for cathode materials. Due to the relatively high phase formation temperature of NVP, it is difficult to obtain NVP particles with both a high crystallinity and nanosized characteristics. (ii) a carbon coating/composite to improve the electrical conductivity.[24-27] Jiang et al. designed core-shell nanostructures with a double carbon coating, and the capacity reached 78 mAh g^{-1} at 30 C.[28] Nie et al. encapsulated NVP in interconnected carbon nanosheets, and a capacity of 46.8 mAh g^{-1} was preserved at 10 C.[29] Compared with other types of carbon, graphene is a single-atomic layer of sp2-bonded carbon atoms that are arranged in a honeycomb crystal structure,[30] which provide a high electronic conductivity.[31-33] Many researchers have also confirmed that enwrapping nanoparticles within graphene sheets to form core-shell

[a] School of Chemistry & Chemical Engineering, South China University of Technology, Guangzhou 510640, China.
[b] School of Chemical Engineering, the University of Adelaide, Adelaide, SA 5005, Australia. E-mail: hhwang@scut.edu.cn; cesqwang@scut.edu.cn

† Footnotes relating to the title and/or authors should appear here.
Electronic Supplementary Information (ESI) available: [details of any supplementary information available should be included here]. See DOI: 10.1039/x0xx00000x

structures can effectively accommodate the volume change and improve the performance of electrode materials.[34-40] However, traditional carbon-coated technology cannot completely prevent particle agglomeration or particle growth, and it usually results in insufficient carbon coating during high temperature calcination, leading to a large polarization that would affect the electrochemical performance of NVP, especially for a supercapacitor-like rate performance.

In this work, we introduced a new strategy to synthesize highly crystalline NVP nanoparticles with a thin carbon-coating layer that is embedded in a three-dimensional (3D) graphene network (donated as NVP@C/G) (as shown in Fig. 1). Through double restrictions of the carbon coating layer and the 3D graphene network, the size of the highly crystalline NVP particles could be maintained at the nanoscale during high temperature sintering. Additionally, the 3D graphene network acts to reinforce the core-shell structure of the NVP@C, thus improving the electrical conductivity of the whole electrode.[34] The designed NVP@C/G exhibits an excellent C-rate capability (76 mAh g^{-1} at 60 C) and a stable cycling performance (82% capacity retention for 1500 cycles at 40 C). The excellent electrochemical performance occurs for three reasons: i) NVP nanoparticles with a high crystallinity shorten the length of the ion/electron transportation and produce a highly electrochemical reaction; ii) the porous structure provides a large active surface area and rich nanopores for the high efficiency electrochemical reaction and fast electrolyte penetration/diffusion; iii) the combined action of the thin carbon coating layer and the interconnected 3D graphene network not only enhances the surface conductivity and electrical contact in the electrode but also buffers the strain and maintains a stable structure during cycling.

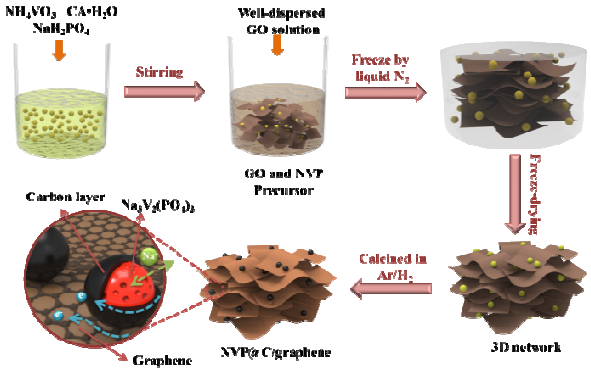

Fig. 1 Schematic diagram of the synthesis process of 3D porous NVP@C/G.

Experimental

Material synthesis

Graphene oxide (GO) was prepared using a modified Hummers method, and the details of the preparation procedure are provided in our previous work.[38] First, NH_4VO_3 (99.9%, Fuchen Chemical Reagents Factory, China), citric acid (99.9%, Sinopharm Chemical Reagent Co., Ltd, China) and NaH_2PO_4 (99.9%, Sinopharm Chemical Reagent Co., Ltd, China) in a 2:2:3 stoichiometric ratio were dissolved in a well-dispersed GO solution. The ingredients were uniformly mixed at the molecular level during this procedure. Here, the citric acid is used as both chelating agent and as a carbon source to generate carbon-coating layers on the NVP particles. Then, the mixture was rapidly frozen via liquid nitrogen, followed by freeze-drying for 48 h. The obtained dry precursor was annealed at different temperatures in the range of 700-900 °C under an Ar/H_2 atmosphere with 8% H_2 (v/v) for 6 h, designated as 700-NVP@C/G, 800-NVP@C/G and 900-NVP@C/G, respectively. For comparison, a control 900-NVP@C sample was also prepared using the same process, except no graphene was added.

Material characterization

Phase analysis was conducted via X-ray diffraction (XRD, Bruker D8 Advance) using Cu-Ka radiation (10 °≤2θ≤60 °) that was operated at 40.0 KV and 40 mA. The morphology was characterized using both scanning electron microscopy (Hitachi SU8000) and transmission electron microscopy (JEOL 2100F). The elemental analysis was performed using an Elementar Vario EL ⍰ elemental analyzer. Thermogravimetric analysis was performed on a NETZSCH STA44C from 25 to 900 °C in air at a heating rate of 10 °C min^{-1}. Raman spectra were measured using a Horiba Jobin Yvon LabRam Aramis Raman spectrometer with a laser of 632.8 nm. The specific surface area was measured using the Brunauere Emmette Teller (BET) method (Micromeritics analyzer ASAP 2020 (USA)) at liquid nitrogen temperature.

Electrochemical characterization

The electrochemical performances were investigated using CR2032 coin cells. The electrodes were fabricated by mixing 80 wt% NVP@C/G, 10 wt% super P (99.9%, Sinopharm Chemical Reagent Co., Ltd, China) and 10 wt% PVDF (99.9%, Sinopharm Chemical Reagent Co., Ltd, China) in N-methyl-2-pyrrolidone (NMP, 99.9%, Sinopharm Chemical Reagent Co., Ltd, China) solvent, and they were laminated onto the aluminum foils. To exclude the influence of the carbon content, the NVP@C electrode was fabricated by mixing with 26 wt% super P and 10 wt% PVDF. The mass loading of the active material was approximately 1.5 mg. Sodium metal (99.0%, Sinopharm Chemical Reagent Co., Ltd, China) was used as the anode. We used 1 M $NaClO_4$ (99.9%, Aladdin Industrial Inc., China) in ethylene carbon (EC, 99.9%, Capchem Inc., China)-diethyl carbonate (DEC, 99.9%, Capchem Inc., China) (1:2 v/v) with 2% FEC (99.9%, Aladdin Industrial Inc., China) as the electrolyte. A glass microfiber filter (Whatman, Grade GF/F) was used as a separator. The discharge and charge measurements were conducted on a NEWWARE battery test system (Shenzhen, China) at a voltage range of 2.5-4.0 V versus Na^+/Na. Cyclic voltammetry was conducted at different scan rates on an electrochemical workstation (CHI660D, Shanghai, China). Electrochemical impedance spectroscopy (EIS) was performed using an electrochemical workstation (Zahner IM6ex) in the frequency range of 100 kHz to 0.01 Hz and at a potential perturbation of 5 mV.

Results and discussion

The X-ray diffraction (XRD) patterns of the three NVP@C/G samples with graphene are shown in Fig. 2a, and the NVP@C sample is shown in Fig. S1†. All of the diffraction peaks in the XRD patterns are indexed to the R-3c space group, and they are in good agreement with the reported literature values of the rhombohedral NASICON framework.[18] The peak intensities increase as the calcination temperature increases, indicating that highly crystalline NVP particles can be achieved at a high sintering temperature. Furthermore, no peaks related to rGO can be observed, indicating that the stacking of the graphene sheets in the NVP@C/G nanocomposites is disordered.[41] The morphologies and detailed structures of the synthesized samples were characterized using scanning electron microscopy (SEM). The SEM images (Fig. 2b-2d) of the NVP@C/G samples illustrate that 3D porous NVP@C/G nanocomposites are obtained, and the NVP nanoparticles are distributed uniformly on the graphene sheets with curled and wavy structures. The graphene matrix provides a 3D conductive network for fast electron transport. The SEM images of NVP@C without graphene (Fig. S2a) show that the NVP particles aggregate and grow to become micron-sized particles during the high temperature treatment. The particle size of NVP@C is randomly distributed within the range of 1-2 μm. The results reveal that the graphene sheets between the NVP nanoparticles effectively restrict the agglomeration and grain growth of the NVP particles. There is no apparent change between 700-NVP@C/G and 800-NVP@C/G. However, upon reaching a calcination temperature of up to 900°C, the edge of the NVP particles in 900-NVP@C/G becomes sharper (Fig. 2d), exhibiting a higher crystallinity than the samples sintered at 700 and 800 °C. This is in accordance with the XRD results.

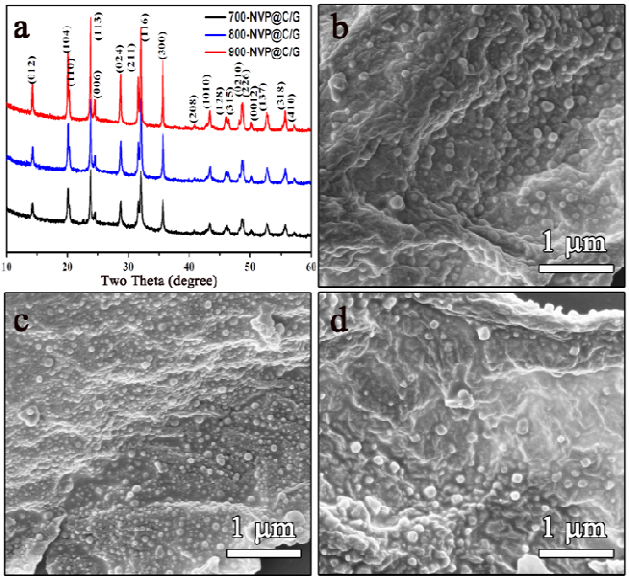

Fig. 2 XRD patterns (a) and SEM images of the 3D porous NVP@C/G nanocomposites that were calcinated at (b) 700 °C, (c) 800 °C and (d) 900 °C.

The distribution and particle sizes of the NVP particles were clearer in the transmission electron microscopy (TEM) images. Fig. 3a-c show that the NVP@C nanoparticles are successfully enwrapped in wrinkled paper-like graphene without distinct agglomeration. The particle size of the NVP@C was well-controlled during the thermal treatment. Even when calcinated at an extremely high temperature (900°C), the size of the highly crystallized NVP particles was well-controlled (<200 nm), and the edge of the NVP particles in the 900-NVP@C/G becomes sharper (Fig. 3c). Compared with the 700-NVP@C/G and 800-NVP@C/G samples (Fig. S3†), the HRTEM images of 900-NVP@C/G (Fig. 3d) also reveal clearer lattice fringes with d-spacing of approximately 0.25 nm that correspond to the (300) lattice planes of NVP with a NASICON structure, indicating the higher crystallinity of 900-NVP@C/G. This result also agrees with the XRD and SEM results. A uniform carbon-coating layer can be clearly observed on the particle surface, and the thickness is approximately 4 nm for 900-NVP@C/G (Fig. 3d). The thin carbon layer on the particle surface combined with the 3D graphene network provides a double restriction on the aggregation of the NVP particles and a 3D highway network for fast electron transport.

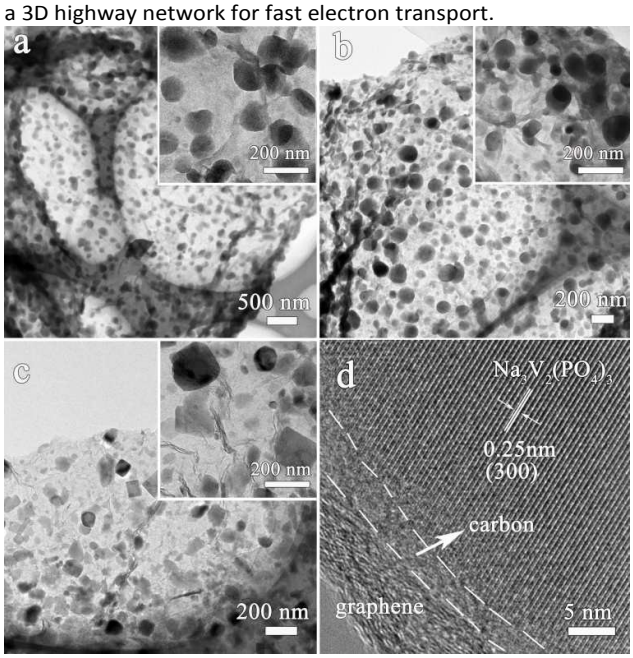

Fig. 3 TEM images of the (a) 700-NVP@C/G, (b) 800-NVP@C/G and (c) 900-NVP@C/G (inset: TEM images at greater magnification) samples. (d) HRTEM image of the 900-NVP@C/G sample.

The carbon content was determined via elemental analysis. The results were 4.59 wt%, 21.96 wt%, 20.58 wt% and 18.34 wt% for 900-NVP@C, 700-NVP@C/G, 800-NVP@C/G and 900-NVP@C/G, respectively (Table S1†). The results are in good agreement with the thermogravimetry (TG) analysis (Fig. S4†). The increasing region in the TG curve is due to the oxidation of V^{3+} in the NVP to V^{4+} and V^{5+}.[28,42] The nitrogen isotherm adsorption/desorption curves and the pore size distributions of NVP@C and NVP@C/G nanocomposites are shown in Fig. S5. All of the four samples exhibit a type IV isotherm with a type-H3 hysteresis loop, demonstrating the presence of a micro/mesoporous structure with a wide range. A pore size peak at 1.3 nm was observed on the pore-size distribution curves of the four samples, which was caused by freeze-

Journal Name

COMMUNICATION

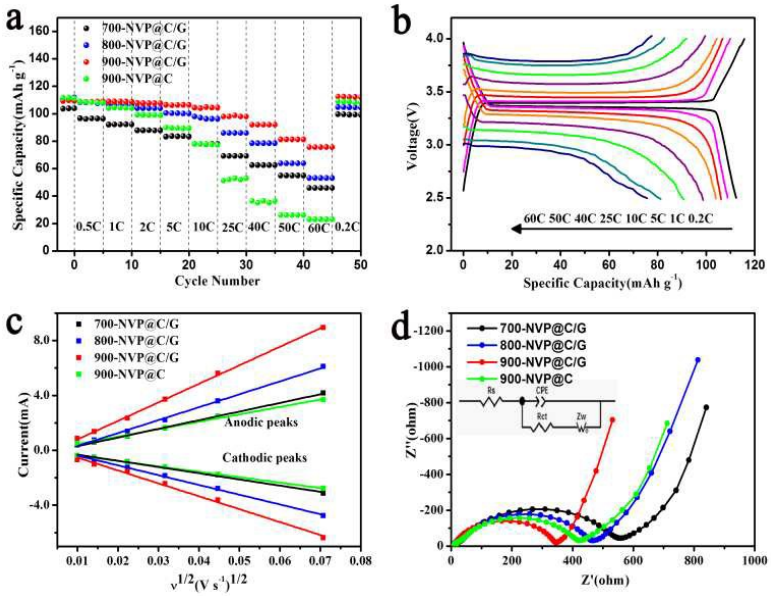

Fig. 4 Electrochemical behaviors: (a) The discharge capacity of 900-NVP@C, 700-NVP@C/G, 800-NVP@C/G and 900-NVP@C/G at different C-rates (0.2-60 C). (b) Representative discharge-charge curves of the 900-NVP@C/G electrode at different C-rates (0.2-60 C). (c) The corresponding relationship between the square root of the scan rate $v^{1/2}$ and the peak current. (d) Nyquist plots of 900-NVP@C, 700-NVP@C/G, 800-NVP@C/G and 900-NVP@C/G (inset: equivalent circuit).

drying.[41] The porous structure is beneficial for the penetration of the electrolyte, and it expands the contact area between the electrode and electrolyte, both of which can facilitate the ultrafast diffusion of Na+ during the sodiation/desodiation process. This contributes to the improvement of the electrochemical performance.[41,43] The BET specific surface area of the 700-NVP@C/G, 800-NVP@C/G and 900-NVP@C/G were calculated to be 118.1, 153.0 and 143.7 m2 g-1, respectively, which are all much higher than that of the 900-NVP@C without graphene (57.9 m^2 g^{-1}). Raman spectra were recorded to further investigate the product compositions (Fig. S6†). The group of peaks observed at 1327 and 1587 cm^{-1} in the four samples can be assigned to the disorder-induced phonon mode (D band) and graphite band (G band), respectively, suggesting the existence of carbon in all of the materials.[43] The intensity ratios of the D band to the G band (I_D / I_G) are 1.47, 1.61, 1.59 and 1.60 for the 900-NVP@C, 700-NVP@C/G, 800-NVP@C/G and 900-NVP@C/G samples, respectively. Additionally, a weak peak at approximately 2650 cm^{-1} is also observed in the 700-NVP@C/G, 800-NVP@C/G and 900-NVP@C/G samples, which is typically assigned as the 2D band of reduced graphene oxide.[39] Obviously, the I_D/I_G ratios of all of the NVP@C/G samples are higher than that of NVP@C, indicating that more defects and edge plane exposure exist in the NVP@C/G, which is caused by the addition of graphene.[26]

The electrochemical behaviors of the NVP@C/G samples and the NVP@C as the cathode for a SIB were evaluated. Because of the 3D conductive network and the high crystallinity of the NVP particles, the 900-NVP@C/G electrode exhibited a very impressive rate capability. The specific discharge capacities were 112, 109, 109, 108, 106, 104, 98 and 92 mAh g^{-1} at current rates of 0.2, 0.5, 1, 2, 5, 10, 25 and 40 C (1 C=117 mA g^{-1}), respectively (Fig. 4a). More impressively, the 900-NVP@C/G cathodes were able to retain a capacity of 81 and 76 mAh g^{-1} even at extremely high rates of 50 C and 60 C, respectively. When the current rate was increased from 0.2 C to 60 C, a high capacity retention of 67.9% was obtained, demonstrating the excellent rate capability. These capacity values are referred to the mass of the NVP and exclude the mass of carbon, which has no contribution in the capability. Fig. 4b shows the charge/discharge curves of 900-NVP@C/G at current rates of 0.2-60 C over a potential window of 2.5-4.0 V. There is a flat voltage plateau at the potential of approximately 3.4 V at the initial lower rate of 0.2 C, corresponding to a reversible phase transformation between $Na_3V_2(PO_4)_3$/$NaV_2(PO_4)_3$, which is also in good agreement with the CV results. Even at 60 C, the voltage plateau was still distinct. However, if there was no support for the 3D graphene network, the voltage plateau was inconspicuous when the current reached 40 C (Fig. S7†). This excellent rate capability is quite superior compared with recent values in the literature.[18-29,42-44]

Journal Name

COMMUNICATION

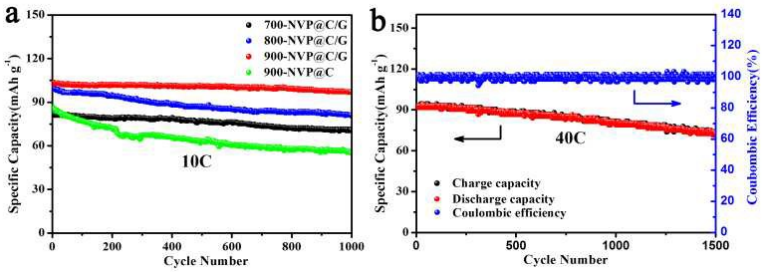

Fig. 5 (a) Cyclic performance of 900-NVP@C, 700-NVP@C/G, 800-NVP@C/G and 900-NVP@C/G at 10 C. (b) Ultralong cyclic performance of 900-NVP@C/G at 40 C.

To further investigate the factors affecting the rate capability, the cyclic voltammogram (CV) curves of the four samples at different scanning rates were obtained (Fig. S8†). The well-defined sharp redox peaks is attributed to the phase transformation of $Na_3V_2(PO_4)_3$ to $NaV_2(PO_4)_3$. The well-defined redox reaction peaks are still maintained even when the scanning rate is as high as 5 mV s^{-1}. The symmetry of the oxidation and reduction peaks in the CV curves confirm the good reversibility of the Na extraction/insertion reactions in these materials.[27] Fig. 4c shows the correlation between the peak current and the square roots of the scan rate for all of the electrodes, which matches the linear relationship very well. This is the typical behavior of a diffusion-controlled electrode reaction process.[40] The diffusion coefficient can be estimated based on the slope of the oblique line,[44,45] and it is easily deduced that the 900-NVP@C/G has the largest Na^+ diffusion coefficient (Table S2†). The high Na^+ diffusion coefficient of 900-NVP@C/G is ascribed to the high degree of crystallinity of NVP nanoparticles, the large surface area of the porous structure and the 3D conductive graphene network. Electrochemical impedance spectroscopic (EIS) measurements were also performed to evaluate the conductivity and diffusion ability of the as-synthesized 900-NVP@C, 700-NVP@C/G, 800-NVP@C/G and 900-NVP@C/G electrodes (Fig. 4d). The Nyquist plots were collected for the frequency range of 10^6 Hz to 10^{-2} Hz at discharge states after 30 charge/discharge cycles. The entire Nyquist plots exhibit a semicircle in the high-frequency region and a straight line in the low-frequency region. The charge transfer resistance (R_{ct}) of the four samples is listed in Table S3†, and the charge transfer resistance of 900-NVP@C was relatively low due to the high crystallinity of the NVP particles and the high carbon black additive (26%) of the 900-NVP@C electrode in the electrode fabrication process. The 900-NVP@C/G electrode shows the lowest charge transfer resistance, implying that the high crystallinity of the NVP nanoparticles and 3D conductive network both facilitate the transport of electrons and sodium ions, which is beneficial for the rate capability.

The cyclic performances of the 900-NVP@C, 700-NVP@C/G, 800-NVP@C/G and 900-NVP@C/G electrodes at a rate of 10 C were also investigated (Fig. 5a). The 900-NVP@C/G electrode exhibits the best cycling performance. It delivers an impressive initial value of 102.3 mAh g^{-1} at a 10 C charge/discharge rate, and it stabilizes at 97.2 mAh g^{-1} after 1000 cycles (corresponds to a capacity retention of 95.0%). For comparison, the 700-NVP@C/G and 800-NVP@C/G cathodes also deliver high reversible capacities of 70.9 mAh g^{-1} and 81.5 mAh g^{-1} after 1000 cycles at 10 C, respectively. However, the 900-NVP@C electrode with high crystallinity NVP nanoparticles and a high carbon additive (26%) exhibits an high initial value of 85.6 mAh g^{-1}, but it only maintains a 64.8% capacity retention after 1000 cycles because of the poor structure stability without graphene's support. Additionally, for a higher rate of up to 40 C, the 900-NVP@C/G could still exhibit great cycling stability (Fig. 5b). The specific capacity is at 86.5 mAh g^{-1}, and only 5.6% of the initial capacity is lost after 500 cycles. Even after 1000 and 1500 cycles, it retains a capacity of 89.0% and 82.0% of its original value. The long cycling stability of 900-NVP@C is attributed to the stable structure, and the carbon-coated NVP nanoparticles enclosed by the graphene sheet maintain a stable structure that suppresses particle agglomeration and buffers the strain during the long sodiation/desodiation process. To our knowledge, such a superior cycling stability has been hard to achieve in prior studies (Table S4†).

Conclusions

We proposed a freeze-drying-assisted thermal treatment method to synthesize 3D NVP@C/G nanocomposites in which NVP nanoparticles with a thin carbon layer were dispersed uniformly on graphene sheets. Thus, both the 3D conductive graphene support network and the carbon-coated structure effectively enhance the electronic conductivity of NVP@C/G. Because of the restriction of the carbon layer and 3D graphene network, the size of the NVP particles were kept at the nanoscale under extremely high temperature calcinations, and highly crystalline particles without agglomeration were

obtained. The optimized 900-NVP@C/G materials exhibits a high Na^+ diffusion coefficient and a low charge transfer resistance due to the high crystallinity of the NVP nanoparticles and the 3D conductive network. Therefore, a superior rate capability and an ultralong cyclability were achieved. Additionally, this easy preparation method provides a broad new strategy to synthesize high crystallinity nanomaterials with a high electronic conductivity and a highly stable structure.

Acknowledgements

The authors greatly acknowledge the financial support of the National Science Fund for Distinguished Young Scholars of China (No. 21225625), the Natural Science Foundation of China (No. 21306057 and 21576100), the Nature Science Foundation of Guangdong (2014A030312007), and the Australian Research Council (ARC) through the Future Fellow Program (FT140100757).

References

1. M. D. Slater, D. Kim, E. Lee and C. S. Johnson, *Adv. Funct. Mater.*, 2013, **23**, 947-958.
2. H. Pan, Y.-S. Hu and L. Chen, *Energy Environ. Sci.*, 2013, **6**, 2338-2360.
3. N. Yabuuchi, M. Kajiyama, J. Iwatate, H. Nishikawa, S. Hitomi, R. Okuyama, R. Usui, Y. Yamada and S. Komaba, *Nat. mater.*, 2012, **11**, 512-517.
4. L. Wang, Y. Lu, J. Liu, M. Xu, J. Cheng, D. Zhang and J. B. Goodenough, *Angew. Chem. Int. Ed.*, 2013, **52**, 1964-1967.
5. V. Palomares, P. Serras, I. Villaluenga, K. B. Hueso, J. Carretero-González and T. Rojo, *Energy Environ. Sci.*, 2012, **5**, 5884-5901.
6. S. P. Ong, V. L. Chevrier, G. Hautier, A. Jain, C. Moore, S. Kim, X. Ma and G. Ceder, *Energy Environ. Sci.*, 2011, 4, 3680-3688.
7. S. W. Kim, D. H. Seo, X. Ma, G. Ceder and K. Kang, *Adv. Energy Mater.*, 2012, **2**, 710-721.
8. V. Palomares, M. Casas-Cabanas, E. Castillo-Martínez, M. H. Han and T. Rojo, *Energy Environ. Sci.*, 2013, **6**, 2312-2337.
9. S. Li, Y. Dong, L. Xu, X. Xu, L. He and L. Mai, *Adv. Mater.*, 2014, **26**, 3545-3553.
10. Y. Yamada, T. Doi, I. Tanaka, S. Okada and J.-i. Yamaki, *J. Power Sources*, 2011, **196**, 4837-4841.
11. Y. Fang, L. Xiao, J. Qian, X. Ai, H. Yang and Y. Cao, *Nano Lett.*, 2014, **14**, 3539-3543.
12. K. T. Lee, T. Ramesh, F. Nan, G. Botton and L. F. Nazar, *Chem. Mater.*, 2011, **23**, 3593-3600.
13. R. Shakoor, D.-H. Seo, H. Kim, Y.-U. Park, J. Kim, S.-W. Kim, H. Gwon, S. Lee and K. Kang, *J. Mater. Chem.*, 2012, **22**, 20535-20541.
14. B. M. de Boisse, D. Carlier, M. Guignard and C. Delmas, *J. Electrochem. Soc.*, 2013, **160**, A569-A574.
15. K. Chihara, A. Kitajou, I. D. Gocheva, S. Okada and J.-i. Yamaki, *J. Power Sources*, 2013, **227**, 80-85.
16. D. Su and G. Wang, *ACS nano*, 2013, **7**, 11218-11226.
17. S. Tepavcevic, H. Xiong, V. R. Stamenkovic, X. Zuo, M. Balasubramanian, V. B. Prakapenka, C. S. Johnson and T. Rajh, *ACS nano*, 2011, **6**, 530-538.
18. K. Saravanan, C. W. Mason, A. Rudola, K. H. Wong and P. Balaya, *Adv. Energy Mater.*, 2013, **3**, 444-450.
19. W. Song, X. Ji, Z. Wu, Y. Zhu, Y. Yang, J. Chen, M. Jing, F. Li and C. E. Banks, *J. Mater. Chem. A*, 2014, **2**, 5358–5362.
20. Z. Jian, L. Zhao, H. Pan, Y.-S. Hu, H. Li, W. Chen and L. Chen, Electrochem. Commun., 2012, **14**, 86-89.
21. Z. Jian, W. Han, X. Lu, H. Yang, Y. S. Hu, J. Zhou, Z. Zhou, J. Li, W. Chen and D. Chen, *Adv. Energy Mater.*, 2013, **3**, 156-160.
22. J. Kang, S. Baek, V. Mathew, J. Gim, J. Song, H. Park, E. Chae, A. K. Rai and J. Kim, *J. Mater. Chem.*, 2012, **22**, 20857-20860.
23. W. Song, X. Cao, Z. Wu, J. Chen, K. Huangfu, X. Wang, Y. Huang and X. Ji, *Phys. Chem. Chem. Phys.*, 2014, **16**, 17681-17687.
24. C. Zhu, K. Song, P. A. van Aken, J. Maier and Y. Yu, *Nano Lett.*, 2014, **14**, 2175-2180.
25. W. Duan, Z. Zhu, H. Li, Z. Hu, K. Zhang, F. Cheng and J. Chen, *J. Mater. Chem. A*, 2014, **2**, 8668-8675.
26. W. Shen, C. Wang, Q. Xu, H. Liu and Y. Wang, *Adv. Energy Mater.*, 2015, **5**, 1400982.
27. J. Liu, K. Tang, K. Song, P. A. van Aken, Y. Yu and J. Maier, *Nanoscale*, 2014, **6**, 5081-5086.
28. Y. Jiang, Z. Yang, W. Li, L. Zeng, F. Pan, M. Wang, X. Wei, G. Hu, L. Gu and Y. Yu, *Adv. Energy Mater.*, 2015, **5**, 1402104.
29. P. Nie, Y. Zhu, L. Shen, G. Pang, G. Xu, S. Dong, H. Dou and X. Zhang, *J. Mater. Chem. A*, 2014, **2**, 18606-18612.
30. C. H. Lui, L. Liu, K. F. Mak, G. W. Flynn and T. F. Heinz, *Nature*, 2009, **462**, 339-341.
31. Y. Sun, Q. Wu and G. Shi, *Energy Environ. Sci.*, 2011, **4**, 1113-1132.
32. D. Chen, H. Feng and J. Li, *Chem. Rev.*, 2012, **112**, 6027-6053.
33. G. Kucinskis, G. Bajars and J. Kleperis, *J. Power Sources*, 2013, **240**, 66-79.
34. W. Wei, S. Yang, H. Zhou, I. Lieberwirth, X. Feng and K. Müllen, *Adv. Mater.*, 2013, **25**, 2909-2914.
35. D. Chen, G. Ji, Y. Ma, J. Y. Lee and J. Lu, *ACS Appl. Mater. Interfaces*, 2011, **3**, 3078-3083.
36. W. Zhou, J. Zhu, C. Cheng, J. Liu, H. Yang, C. Cong, C. Guan, X. Jia, H. J. Fan and Q. Yan, *Energy Environ. Sci.*, 2011, **4**, 4954-4961.
37. J. Luo, J. Liu, Z. Zeng, C. F. Ng, L. Ma, H. Zhang, J. Lin, Z. Shen and H. J. Fan, *Nano Lett.*, 2013, **13**, 6136-6143.
38. P. Lian, X. Zhu, S. Liang, Z. Li, W. Yang and H. Wang, *Electrochim. Acta*, 2010, **55**, 3909-3914.
39. Y. H. Jung, C. H. Lim and D. K. Kim, *J. Mater. Chem. A*, 2013, **1**, 11350-11354.
40. N. Mahmood, C. Zhang, H. Yin and Y. Hou, *J. Mater. Chem. A*, 2014, **2**, 15-32.
41. D. Cai, P. Lian, X. Zhu, S. Liang, W. Yang and H. Wang, *Electrochim. Acta*, 2012, **74**, 65-72.
42. K. Du, H. Guo, G. Hu, Z. Peng and Y. Cao, Journal of Power Sources, 2013, 223, 284-288.
43. W. Shen, C. Wang, H. Liu and W. Yang, *Chem. Eur. J.*, 2013, **19**, 14712-14718.
44. W. Song, X. Ji, Y. Yao, H. Zhu, Q. Chen, Q. Sun and C. E. Banks, *Phys. Chem. Chem. Phys.*, 2014, **16**, 3055-3061.
45. G. Li, D. Jiang, H. Wang, X. Lan, H. Zhong and Y. Jiang, *J. Power Sources*, 2014, **265**, 325-334.

We introduced a new strategy to synthesize NVP nanoparticles with a thin carbon-coating layer embedded in three-dimensional (3D) graphene network.